

Study of orbitally excited ($L = 1$) B mesons

The CDF Collaboration

Version 0.1, September 13, 2007

Abstract

We report a measurement of the masses and width of the neutral orbitally excited B mesons in decays to $B^{(*)+}\pi^-$ using 1.7 fb^{-1} of data collected by the CDF II detector at the Fermilab Tevatron. The mass and width of the narrow B_2^{*0} state are measured to be $m(B_2^{*0}) = 5739.9_{-1.8}^{+1.7}$ (stat.) $_{-0.6}^{+0.5}$ (syst.) MeV/c^2 and $\Gamma(B_2^{*0}) = 22.1_{-3.1}^{+3.6}$ (stat.) $_{-2.6}^{+3.5}$ (syst.) MeV/c^2 respectively. The mass difference between the narrow B_2^{*0} and B_1^0 states is measured to be $14.6_{-2.5}^{+2.2}$ (stat.) $_{-0.9}^{+0.7}$ (syst.) MeV/c^2 , resulting in a B_1^0 mass of $5725.3_{-2.1}^{+1.6}$ (stat.) $_{-1.1}^{+0.8}$ (syst.) MeV/c^2 . This is currently the most precise mass measurement of the narrow B^{**0} states and the first measurement of the B_2^{*0} width.

The B meson consists of a heavy b quark bound to a light u or d quark. The ground $J^P = 0^-$ (B) and 1^- (B^*) states are well established [1], but the spectroscopy of the excited B states has not been well studied. The first excited state of the B meson is predicted to occur when the light quark has an orbital angular momentum of $L = 1$. This results in two isodoublets of excited states, one with a light quark angular momentum of $J_l = \frac{1}{2}$ and a total angular momentum of $\mathbf{J} = 0$ (B_0^*) or 1 (B_1), and another with $J_l = \frac{3}{2}$, $\mathbf{J} = 1$ (B_1) or 2 (B_2^*) [2–5]. The four states are collectively referred to as B^{**} . The $J_l = \frac{1}{2}$ states decay to $B^{(*)}\pi$ via an S -wave transition. Consequently, these states are expected to be very broad and have not yet been observed. The $J_l = \frac{3}{2}$

23 states decay to $B^{(*)}\pi$ via a D -wave transition and are expected to have widths of
24 $10 - 20 \text{ MeV}/c^2$ [3]. The decay $B_1 \rightarrow B\pi$ is forbidden by angular momentum and
25 parity conservation, while both $B_2^* \rightarrow B\pi$ and $B_2^* \rightarrow B^*\pi$ decays are allowed.

26 Previous measurements of the neutral B_1 and B_2^* states have been made using
27 inclusive or semi-inclusive decays which did not allow for separation of the narrow
28 states [6–11], or were statistically limited [12]. Recently the neutral B_1 and B_2^* states
29 were observed separately by the DØ Collaboration [13], but the width of the narrow
30 states was not measured. In this Letter, we present a measurement of the masses of
31 the two $J_l = \frac{3}{2}$ B^{**0} states and a measurement of the width of the B_2^{*0} state. We
32 reconstruct B^{**0} in $B^+\pi^-$ and $B^{*+}\pi^-$ decays; throughout this paper, any reference to
33 a specific charge state implies the charge conjugate state as well. We use data collected
34 by the CDF II Detector at the Fermilab Tevatron between February 2002 and January
35 2007, corresponding to a total integrated luminosity of 1.7 fb^{-1} .

36 The components of the CDF II detector [14] used for this analysis are the magnetic
37 spectrometer and the muon detectors. The tracking system is composed of a silicon
38 microstrip detector [15] able to measure impact parameters with a resolution on the
39 order of $35 \text{ }\mu\text{m}$ [16]. It is surrounded by an open-cell drift chamber (COT) [17]. Both
40 components are located inside a 1.4 T axial magnetic field. Muons are detected in
41 planes of multi-wire drift chambers and scintillators [18] in the pseudorapidity range
42 $|\eta| \leq 1.0$, where $\eta = -\ln \tan(\theta/2)$ and θ is the polar angle measured from the proton
43 direction.

44 A three-level trigger system is used for the online event selection. The important
45 trigger components for this analysis are the Extremely Fast Tracker (XFT) [19], which
46 finds tracks in the COT in the level 1 trigger, and the Silicon Vertex Trigger (SVT) [20],
47 which at level 2 adds information from the silicon detector to the tracks found by the
48 XFT. Two independent level 3 triggers are used in this analysis. The dimuon trigger
49 [14] requires two tracks of opposite charge matched to track segments in the muon

50 chambers, where the mass of the pair is consistent with the J/ψ mass. The displaced
 51 vertex trigger [21] requires two tracks with large impact parameters. Additionally, the
 52 intersection of the tracks must be displaced from the interaction point and a minimum
 53 transverse momentum, the momentum component perpendicular to the proton beam
 54 direction, is required for each track.

55 The offline reconstruction begins by reconstructing B^+ candidates in the $J/\psi K^+$,
 56 $\bar{D}^0 \pi^+$, and $\bar{D}^0 \pi^+ \pi^+ \pi^-$ decay modes with $J/\psi \rightarrow \mu^+ \mu^-$ and $\bar{D}^0 \rightarrow K^+ \pi^-$. Decays
 57 of $B^+ \rightarrow J/\psi K^+$ are reconstructed from the dimuon trigger data while decays of
 58 $B^+ \rightarrow \bar{D}^0 \pi^+ (\pi^+ \pi^-)$ are reconstructed from the displaced vertex trigger data. In
 59 all three decay modes, the tracks are constrained to the appropriate vertex topology
 60 with the J/ψ and \bar{D}^0 masses constrained to the world average values [1]. All tracks
 61 not used to reconstruct a B^+ candidate are considered pion candidates and combined
 62 with B^+ candidates to form B^{**} candidates. We search for narrow resonances in the
 63 mass difference distribution of $Q = m(B^+ \pi^-) - m(B^+) - M_{\pi^-}$, where $m(B^+ \pi^-)$ and
 64 $m(B^+)$ are the reconstructed invariant masses of the $B^+ \pi^-$ pair and the B^+ candidate
 65 respectively, and M_{π^-} is the known pion mass [1].

66 Selection of the B^{**} candidates is done using separate neural networks for each of
 67 the three B^+ decay modes. The neural networks are based on the NEUROBAYES [22]
 68 package and combine discriminating variables into a single discriminating quantity.

69 We start by selecting good B^+ candidates for which we build three different neural
 70 networks. Neural networks in the $B^+ \rightarrow J/\psi K^+$ and $B^+ \rightarrow \bar{D}^0 \pi^+ \pi^+ \pi^-$ channels use
 71 simulated events as the signal patterns and data events from the B^+ mass sideband
 72 as the background patterns for training. In the $B^+ \rightarrow \bar{D}^0 \pi^+$ channel, the neural
 73 network is trained using only data. To train on data only, we take B^+ candidates
 74 in the invariant mass signal region of 5240 to 5310 MeV/c^2 as the signal patterns
 75 and B^+ candidates in the invariant mass sideband region of 5325 to 5370 MeV/c^2 as
 76 the background patterns. Events from the B^+ mass sideband are also used as signal

77 patterns with a negative weight to account for the background in the signal region. The
78 most important topological and kinematic discriminants for the neural networks are the
79 impact parameter of the B^+ , the projection of the distance of the B^+ decay vertex to
80 the primary vertex on the normalized transverse momentum, the transverse momentum
81 of the kaon or pion from the B^+ decay, and the impact parameter of the kaon or pion
82 from the B^+ decay. The neural networks for B^+ selection in the $B^+ \rightarrow J/\psi K^+$ and
83 $B^+ \rightarrow \bar{D}^0 \pi^+$ channels are taken from the study of the B_s^{**} states [23]. In total, 51,500
84 B^+ signal events are selected in the $J/\psi K^+$ decay channel, 40,100 in the $\bar{D}^0 \pi^+$ channel,
85 and 11,000 in the $\bar{D}^0 \pi^+ \pi^+ \pi^-$ channel.

86 For the B^{**} selection, three neural networks are trained on a combination of sim-
87 ulated events for the signal patterns and data for the background patterns. The data
88 for the background patterns are taken from the entire Q range of 0 to 1 GeV/ c^2 . The
89 signal contribution in the data is marginal and can be neglected during neural net-
90 work training. To avoid biasing of the neural network training, the simulated events
91 are generated with the same Q distribution as the data. The neural network inputs
92 include the output of the corresponding B^+ neural network and the properties of the
93 pion from B^{**} decay in addition to the quantities used by the corresponding B^+ neural
94 network. The most important discriminants are the impact parameter and transverse
95 momentum of the pion from B^{**} decay and the output of the B^+ neural network.

96 For the final B^{**} selection we select on the number of candidates per event and on
97 the output of the neural networks. The requirement on the number of candidates is
98 fixed to be the same for all three B^+ decay channels, and requires fewer than six B^{**}
99 candidates in an event. The cut on the neural network output is chosen to maximize
100 $N_{MC}/\sqrt{N_{data}}$, which is proportional to the significance $S/\sqrt{S+B}$. The optimization
101 is done by counting the number of Monte Carlo events N_{MC} and the number of data
102 events N_{data} in the Q signal region of 0.2 GeV/ c^2 to 0.4 GeV/ c^2 for a given cut on
103 the network output. In this analysis, we combine the B^{**} events for all three B^+

104 decay channels and use this combined Q distribution to measure the B^{**} properties.
 105 Thus, we optimize the B^{**} selection for each B^+ decay channel using the combined
 106 significance, which is a function of all three network outputs. The best cuts on the
 107 neural network outputs are 0.85 for the decay $B^{**0} \rightarrow B^+\pi^- \rightarrow (J/\psi K^+)\pi^-$, 0.7 for
 108 $B^{**0} \rightarrow B^+\pi^- \rightarrow (\bar{D}^0\pi^+)\pi^-$, and 0.75 for $B^{**0} \rightarrow B^+\pi^- \rightarrow (\bar{D}^0\pi^+\pi^+\pi^-)\pi^-$. The
 109 resulting combined Q distribution is shown in Figure 1.

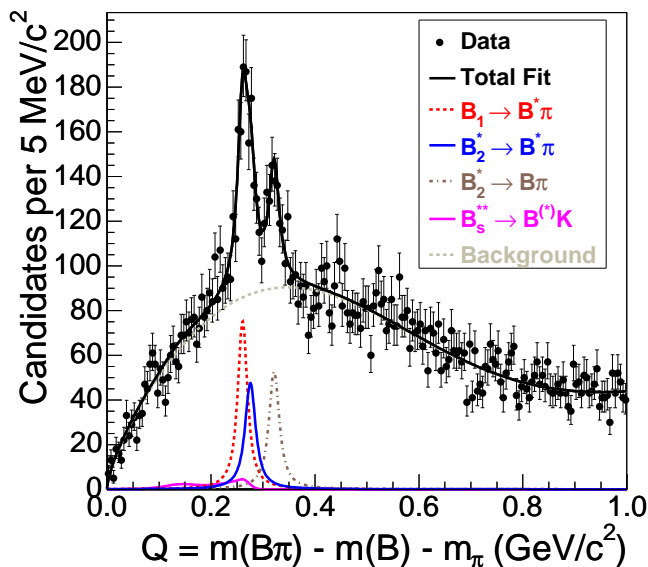


Figure 1: Invariant mass distribution $Q = m(B^+\pi^-) - m(B^+) - M_{\pi^-}$ for exclusive B^+ decays. The fit is described in the text. Curves are shown separately for the background, the B_s^+ reflections, and the three B^{**} decays.

110 We perform an unbinned maximum likelihood fit to the combined Q distribution.
 111 The B^{**} signal structure is interpreted as the three decays $B_1^0 \rightarrow B^{*+}\pi^-$, $B_2^0 \rightarrow B^+\pi^-$,
 112 and $B_2^0 \rightarrow B^{*+}\pi^-$, with $B^{*+} \rightarrow B^+\gamma$, where the photon is not detected. Because of
 113 the missing photon, the observed B_1^0 and $B_2^0 \rightarrow B^{*+}\pi^-$ peaks are shifted to a lower
 114 mass by the $B^* - B$ mass splitting of 45.78 ± 0.35 MeV/ c^2 [1], resulting in three
 115 separate narrow B^{**} signal peaks. Each peak is modeled by a non-relativistic fixed-
 116 width Breit-Wigner distribution convoluted with the detector resolution model. The

117 detector resolution as a function of Q is determined from simulation and modeled by
 118 two Gaussian distributions, a dominant narrow core of an ~ 2 MeV/ c^2 width and a
 119 small broad component of an ~ 4 MeV/ c^2 width for the tails. A systematic uncertainty
 120 is assigned for possible underestimation of the detector resolution by the simulation.

121 The current sample of data has insufficient statistics to fit for all signal parameters.
 122 We fit for the Q value of the $B_2^{*0} \rightarrow B^+\pi^-$ decay, the mass difference between the
 123 B_1^0 and B_2^{*0} states, the width of the B_2^{*0} , and the number of events in the B_1^0 and
 124 $B_2^{*0} \rightarrow B^+\pi^-$ peaks. The parameters taken from theoretical predictions or previous
 125 measurements enter the fit as Gaussian constraints to the likelihood, and are: the
 126 energy of the B^* photon, $E(\gamma) = 45.78 \pm 0.35$ MeV/ c^2 [1]; the ratio of the B_1^0 and B_2^{*0}
 127 widths, $\frac{\Gamma(B_1^0)}{\Gamma(B_2^{*0})} = 0.9 \pm 0.2$ [3]; the ratio of the B_2^{*0} branching fractions, $\frac{BR(B_2^{*0} \rightarrow B^+\pi^-)}{BR(B_2^{*0} \rightarrow B^{*+}\pi^-)} =$
 128 1.1 ± 0.3 , which is based on observations of the charm sector [11].

129 We also expect reflections from $B_s^{**0} \rightarrow B^+K^-$ decays in the B^{**} Q distribution
 130 when the kaon is reconstructed as a pion. The shape of this reflection is determined
 131 using simulations from the study of the B_s^{**} states [23] and is a fixed component of the
 132 fit. The number of B_s^{**0} events expected in the B^{**} distributions is also determined
 133 from [23] and enter the fit as Gaussian constraints with an assigned 50% uncertainty.
 134 In this data sample we expect 24 B_{s1}^0 events and 62 B_{s2}^{*0} events.

135 The background is modeled by a smooth function, a power law times an exponential.
 136 There is a small fixed component to the background at high Q values ($Q > 0.7$ GeV/ c^2),
 137 but the background shape under the B^{**} signal region is allowed to float in the fit to
 138 data. Tests of the fit on randomly generated samples show that it is stable, with
 139 negligible fit bias on the B^{**} signal parameters.

140 The result of this fit to the combined data is shown in Figure 1. The χ^2 probability
 141 of the fit is 78% in the range $Q \in [0.0, 0.5]$ GeV/ c^2 , and 53% over the full range of
 142 $Q \in [0.0, 1.0]$ GeV/ c^2 . The following parameters are measured for the B_1^0 and B_2^{*0} :

143 $m(B_2^{*0}) - m(B^+) - M_{\pi^-} = 321.5_{-1.8}^{+1.7}$ (stat.) $_{-0.3}^{+0.4}$ (syst.) MeV/ c^2

144 $m(B_2^{*0}) - m(B_1^0) = 14.9_{-2.5}^{+2.2}$ (stat.) $_{-0.9}^{+0.7}$ (syst.) MeV/ c^2

145 $\Gamma(B_2^{*0}) = 22.7_{-3.2}^{+3.8}$ (stat.) $_{-1.6}^{+2.1}$ (syst.) MeV/ c^2

146 The number of events are $N(B_1^0) = 503_{-68}^{+75}$ (stat.) $_{-73}^{+86}$ (syst.) and $N(B_2^{*0} \rightarrow B^+\pi^-) =$
 147 385_{-45}^{+48} (stat.) $_{-23}^{+32}$ (syst.). The signal is consistent with theoretical predictions, in-
 148 cluding those entered as Gaussian constraints in the likelihood. Using the mass of the
 149 B^+ [1] and the correlations between the fit parameters, the absolute masses of the B_1^0
 150 and B_2^{*0} are:

151 $m(B_2^{*0}) = 5740.2_{-1.8}^{+1.7}$ (stat.) $_{-0.5}^{+0.6}$ (syst.) MeV/ c^2

152 $m(B_1^0) = 5725.3_{-2.2}^{+1.6}$ (stat.) $_{-1.1}^{+0.9}$ (syst.) MeV/ c^2

153 while the number of $B_2^{*0} \rightarrow B^{*+}\pi^-$ events is found to be 351_{-45}^{+48} (stat.) $_{-23}^{+31}$ (syst.). With
 154 the current statistics, the data is also consistent with having only the B_1^0 and $B_2^{*0} \rightarrow$
 155 $B^+\pi^-$ peaks, so the interpretation of three signal peaks is motivated by theoretical
 156 predictions.

157 Systematic uncertainties on the mass difference and yield measurements fall into
 158 three categories: mass scale, assumptions entered as Gaussian constraints in the fit,
 159 and the choice of background and resolution models.

160 To determine the mass scale uncertainty, we compare CDF II measured Q values
 161 of the D^* , Σ_c^0 , Σ_c^{++} , Λ_c^* , and $\psi(2s)$ hadrons with the world average Q values [1]. The
 162 Q value dependence of this systematic uncertainty is modeled with a linear function,
 163 which is evaluated at the B^{**} Q values to estimate the systematic uncertainty. This is
 164 a small contribution to the systematic uncertainty with a value of about 0.05 MeV/ c^2 .

165 Assumptions made in the fit are included as Gaussian constraints added to the
 166 likelihood. Thus, the systematic uncertainty due to these assumptions is part of the fit

167 uncertainty on each parameter. To separate the statistical and systematic components
 168 of the fit uncertainty, we refit the data with the constrained parameters fixed. The
 169 uncertainty on each parameter from this fit is purely statistical. To determine the
 170 systematic contribution to the fit uncertainty, we subtract in quadrature the uncer-
 171 tainties for the two fits to data, one with the constrained parameters floating and one
 172 with them fixed. Assumptions in the fit are the largest systematic uncertainty on all
 173 parameters, ranging from 30 – 90 on the numbers of events and 0.3 – 1 MeV/ c^2 on the
 174 mass difference measurements.

175 To estimate the uncertainty due to the choice of background or resolution models,
 176 we generate pseudo-experiments using an alternate background parameterization or
 177 increased resolution width. Each pseudo-experiment is modeled by both the default
 178 fit and the fit with an alternate background model or increased resolution width. We
 179 then take the difference between the parameter values in the varied fit and the default
 180 fit as the systematic uncertainty due to these model. We model this difference with
 181 a Gaussian and take the mean of the Gaussian as the systematic uncertainty. The
 182 uncertainty due to the detector resolution underestimation is negligible, causing an
 183 uncertainty of about 2 on the numbers of events and at most 0.003 MeV/ c^2 on the
 184 mass difference measurements. The uncertainty due to the background model is also
 185 relatively small, causing an uncertainty of about 20 on the numbers of events and at
 186 most 0.16 MeV/ c^2 on the mass difference measurements.

187 In summary, using the three fully reconstructed decay modes $B^{**0} \rightarrow B^+\pi^- \rightarrow$
 188 $(J/\psi K^+)\pi^-$, $B^{**0} \rightarrow B^+\pi^- \rightarrow (\bar{D}^0\pi^+)\pi^-$, and $B^{**0} \rightarrow B^+\pi^- \rightarrow (\bar{D}^0\pi^+\pi^+\pi^-)\pi^-$,
 189 we observe the two narrow B^{**0} states in agreement with previous measurements and
 190 theoretical predictions. This is the most precise measurement of the narrow B^{**0} states
 191 to date. This is also the first measurement of the B_2^{*0} width.

192 We thank the Fermilab staff and the technical staffs of the participating institu-
 193 tions for their vital contributions. This work was supported by the U.S. Department of

194 Energy and National Science Foundation; the Italian Istituto Nazionale di Fisica Nu-
195 cleare; the Ministry of Education, Culture, Sports, Science and Technology of Japan;
196 the Natural Sciences and Engineering Research Council of Canada; the National Sci-
197 ence Council of the Republic of China; the Swiss National Science Foundation; the
198 A.P. Sloan Foundation; the Bundesministerium für Bildung und Forschung, Germany;
199 the Korean Science and Engineering Foundation and the Korean Research Foundation;
200 the Science and Technology Facilities Council and the Royal Society, UK; the Institut
201 National de Physique Nucleaire et Physique des Particules/CNRS; the Russian Founda-
202 tion for Basic Research; the Comisión Interministerial de Ciencia y Tecnología, Spain;
203 the European Community's Human Potential Programme; the Slovak R&D Agency;
204 and the Academy of Finland.

205 References

- 206 [1] W. M. Yao *et al.* (Particle Data Group), *J. Phys. G* **33**, 1 (2006).
- 207 [2] E. J. Eichten, C. T. Hill, and C. Quigg, *Phys. Rev. Lett.* **71**, 4116 (1993);
208 E. J. Eichten, C. T. Hill, and C. Quigg, FERMILAB-CONF-94/118-T (1994).
- 209 [3] A. F. Falk and T. Mehen, *Phys. Rev. D* **53**, 231 (1996).
- 210 [4] N. Isgur, *Phys. Rev. D* **57**, 4041 (1998).
- 211 [5] D. Ebert, V. O. Galkin, and R. N. Faustov, *Phys. Rev. D* **57**, 5663 (1998)
212 [Erratum-*ibid.* *D* **59**, 019902 (1999)].
- 213 [6] R. Akers *et al.* (OPAL Collaboration), *Z. Phys. C* **66**, 19 (1995).
- 214 [7] P. Abreu *et al.* (DELPHI Collaboration), *Phys. Lett. B* **345**, 598 (1995).
- 215 [8] D. Buskulic *et al.* (ALEPH Collaboration), *Z. Phys. C* **69**, 393 (1996).

- 216 [9] M. Acciarri *et al.* (L3 Collaboration), Phys. Lett. B **465**, 323 (1999).
- 217 [10] A. A. Affolder *et al.* (CDF Collaboration), Phys. Rev. D **64**, 072002 (2001).
- 218 [11] Z. Albrecht *et al.* (DELPHI Collaboration), DELPHI 2004-025 CONF 700,
219 contributed paper to ICHEP 2004, Beijing.
- 220 [12] R. Barate *et al.* (ALEPH Collaboration), Phys. Lett. B **425**, 215 (1998).
- 221 [13] V. M. Abazov *et al.* (D0 Collaboration), arXiv:0705.3229 [hep-ex].
- 222 [14] D. Acosta *et al.* (CDF Collaboration), Phys. Rev. D **71**, 032001 (2005).
- 223 [15] C. S. Hill, Nucl. Instrum. Methods A **530**, 1 (2004); A. Affolder *et al.*, Nucl.
224 Instrum. Methods A **453**, 84 (2000); A. Sill, Nucl. Instrum. Methods A **447**,
225 1 (2000).
- 226 [16] A. Bardi *et al.*, Nucl. Instrum. Methods Phys. Res. A **485**, 178 (2002).
- 227 [17] T. Affolder *et al.*, Nucl. Instrum. Methods A **526**, 249 (2004).
- 228 [18] G. Ascoli *et al.*, Nucl. Instrum. Methods A **268**, 33 (1988).
- 229 [19] E. J. Thomson *et al.*, IEEE Trans. Nucl. Sci. **49**, 1063 (2002).
- 230 [20] W. Ashmanskas *et al.*, Nucl. Instrum. Methods A **518**, 532 (2004).
- 231 [21] A. Abulencia *et al.* (CDF Collaboration), Phys. Rev. Lett. **96**, 191801 (2006).
- 232 [22] M. Feindt, arXiv:physics/0402093 (2004); M. Feindt and U. Kerzel, Nucl. In-
233 strum. Methods A **559**, 190 (2006).
- 234 [23] CDF Collaboration, “Observation of orbitally excited $L = 1$ B_s mesons”, CDF
235 Note 8468 (2006).